



Fluorescent glutathione probe based on MnO₂–Si quantum dots nanocomposite directly used for intracellular glutathione imaging



Hong Ma^a, Xinran Li^a, Xiaoyu Liu^{a,b}, Min Deng^a, Xudong Wang^a, Anam Iqbal^a, Weisheng Liu^a, Wenwu Qin^{a,*}

^a Key Laboratory of Nonferrous Metal Chemistry and Resources Utilization of Gansu Province and State Key Laboratory of Applied Organic Chemistry,

College of Chemistry and Chemical Engineering, Lanzhou University, Lanzhou 730000, PR China

^b College of Petrochemical Technology, Lanzhou University of Technology, Lanzhou 730050, PR China

ARTICLE INFO

Article history:

Received 6 January 2017

Received in revised form 9 August 2017

Accepted 9 August 2017

Available online 30 August 2017

Keywords:

Silicon quantum dots

Fluorescent probe

Glutathione

Cell culture

Intracellular imaging

ABSTRACT

A highly sensitive glutathione probe based on silicon quantum dots (SiQDs) modified with MnO₂ nanosheets has been developed. A strong reduction of the blue fluorescence of the SiQDs happened due to the surface energy transfer (SET) from SiQDs to the deposited MnO₂. Fluorescence can be restored in the presence of glutathione on account of the MnO₂ nanosheets are reduced. A fluorometric glutathione detection assay with a low detection limit (153 nM, at an S/N ratio of 3) can be designed via this method. It can be applied to directly determine GSH in living cells. A significant blue fluorescence image is produced in the cytosol of the cell and the fluorescence disappears while the cells treated with scavenger of GSH.

© 2017 Elsevier B.V. All rights reserved.

1. Introduction

Glutathione (GSH) is a thiol group containing tripeptide (γ -L-glutamyl-L-cysteinyl-glycine) that plays an important role in an antioxidant defense, nutrient metabolism, and regulation of cellular events (including gene expression, DNA, protein synthesis, cell proliferation and apoptosis, signal transduction, cytokine production and immune response, and protein glutathionylation). While, the abnormal levels of GSH has been proved to be directly linked to various diseases, such as kwashiorkor, seizure, Alzheimers's, Parkinson's, liver, cystic fibrosis, sickle cell anemia, HIV, AIDS, cancer, heart attack, stroke, diabetes and accelerates the aging process [1]. Consequently, the quantitative detection of GSH in biological systems consistently attracts a great deal of attention. Usually, the concentration of GSH in cells is about 0.5–10 mmol L⁻¹ [1].

To date, numerous methods, including fluorescent spectroscopy [2–8], electrochemical pulse voltammetric methods [9–11], high-performance liquid chromatography (HPLC) [12–14], and colorimetric assays [15–17], have been reported for the quantitative detection of GSH. Among the various analytical methods, fluorescence sensing is the most appealing due to its generally non-

destructive character, high sensitivity and easy to use. Recently, Santra et al. reported a simple quantum-dot-based Off-On fluorescent probe for detecting glutathione with high selectivity and sensitivity [18]. However, the toxicity of these quantum dots (QDs) has to be remedied if one wants to design fluorescent GSH probes which are used inside the biological cells, because the QDs contain Cd or other heavy metal ions. A sensitive turn-on sensor for GSH in the cell samples based on the recovered fluorescence of the gold nanoclusters-Hg²⁺ system was reported by Zhu et al. [19]. However, Hg is one kind of well-known toxicity heavy metal and has potential environmental hazard. Cai et al. reported a rapid fluorescence “switch-on” assay for glutathione detection by using carbon dots-MnO₂ nanocomposites but it is only used in human serum samples [20]. So, it is necessary to find a safe and environment friendly fluorescence GSH probe in the cells samples.

Silicon quantum dots (SiQDs) have received extensive attention because of high fluorescence quantum yield (QY), size-dependent multicolor fluorescence by the quantum confinement effect, high photostability in an aqueous solution or an ambient air, good biocompatibility and easy modification to couple with biomolecules. As compared to other QDs, the superior advantage of SiQDs is nontoxic because they are composed of nontoxic elements and have little environmental impact. SiQDs are versatile and tunable surface functionalities, because of their superior properties which distinguish the SiQDs from traditional fluorescence probes. Due to

* Corresponding author. Tel.: +86 931 8912582; fax: +86 931 8912582.

E-mail address: qinww@lzu.edu.cn (W. Qin).

this advantage, SiQDs have extensive explorations in a multitude of exciting areas, ranging from bioimaging [21–23], drug delivery [24,25], catalysis [26,27] and biosensing [28].

Herein, we fabricate a MnO_2 functionalized SiQDs which was prepared by in-situ synthesis of MnO_2 nanosheets in SiQDs solutions (**Scheme 1**). As soon as the MnO_2 –SiQD nanocomposite was formed, the fluorescence of SiQDs in this nanocomposite can be effectively quenched, because the distance between SiQDs and MnO_2 nanosheets is close enough and consequently surface energy transfer (SET) happened. Interestingly, this MnO_2 -induced quenching effect can be recovered in the presence of GSH because of the decomposition of the MnO_2 to Mn^{2+} by GSH. Moreover, the nanocomposites also exhibit high selectivity towards GSH relative to other biomolecules and electrolytes. Finally, the practical use of this nanoprobe for GSH determination in living cells was also presented.

2. Experimental

2.1. Chemicals

KMnO_4 was purchased from Guangfu Reagent Company (Tianjin, China). Ascorbate sodium (AS) was purchased from Sinopharm chemical Regent co. Ltd (Beijing, China). (3-aminopropyl) trimethoxysilane (APTES) (98%) was purchased from Alfa Aesar Company. 4-Morpholineethane sulfonic acid (MES) and *N*-methylleimide were purchased from Energy chemical (Shanghai, China). L-Glutathione, Bovine serum albumin (BSA), D-fructose, cysteine (Cys), ascorbic acid (AA), homocysteine (Hcy), glutamic acid (Glu), glycine (Gly) and D-aspartic acid (Asp) were purchased from Heowns (Tianjing, China). Ultrapure water obtained from a Milli-Q ultrapure ($18.2\text{ M}\Omega\text{ cm}$) system was used in all experiments.

2.2. Instrument

The transmission electron microscopy (TEM) was taken on a JEOL JEM2100 TEM instrument at an accelerating voltage of 120 kV equipped with an energy-dispersive X-ray (EDX) spectrometer. FT-IR spectra were conducted within the 4000–400 cm^{-1} wavenumber range using a Nicolet 360 FTIR spectrometer with the KBr pellet technique. X-ray photoelectron spectra (XPS) was measured on a PHI-550 spectrometer by using Mg Ka radiation ($h\nu = 1253.6\text{ eV}$) photoemission spectroscopy with a base vacuum operated at 300 W. The hydrodynamic diameter and size distribution was measured with dynamic scattered light (DLS) (BI-200SM) at room temperature using water as the solvent. UV–Vis absorption spectra were recorded on a Varian UV-Cary100 spectrophotometer, and for the corrected steady-state fluorescence emission spectra, a FLS920 spectrofluorometer was employed. Fluorescence lifetimes were obtained by a FLS920 spectrometer equipped with a supercontinuum white laser (400–700 nm) and fluorescence decay histograms were recorded using the time-correlated single photon counting technique in 4096 channels and decays were obtained until it typically reached 5.0×10^3 counts. The obtained histograms were fitted as a sum of the exponential, using Gaussian-weighted nonlinear least squares fitting based on Marquardt–Levenberg minimization implemented in the software package of the instrument and the fitting parameters were decided by minimizing the reduced chi-square.

2.3. Synthesis of SiQDs

SiQDs were synthesized according to a reported method [29]. In a typical synthesis, the SiQDs were prepared by adding 1 mL of APTES to 4 mL ultrapure water with constant smooth stirring. Then,

1.25 mL of AS (0.1 M) was added to the above mixture by stirring for 20 min. The total synthesis was completed in 30 min. After storage at room temperature one week, the resulting SiQDs sample exhibited an intense blue fluorescence under UV irradiation.

2.4. Synthesis of MnO_2 –SiQD nanocomposite

In a typical reaction, 750 μL of SiQDs was added to 2.5 mL of MES buffer (0.1 M, pH 6.0). 1 mL KMnO_4 (10 mM) was added and the volume of mixture was adjusted to 10 mL with ultrapure water. After that, the resulting mixture was sonicated for 30 min until a brown colloid was formed. Subsequently, the MnO_2 –SiQD nanocomposite was collected by centrifugation and washed three times with ultrapure water to remove the excess potassium and free manganese ions. The product then was redispersed in 10 mL of ultrapure water.

2.5. Fluorescence sensing of GSH

For the quantitative detection of GSH, the sensing solutions were prepared by mixing 10 μL of MnO_2 –SiQD nanocomposite solutions with 10 μL of different concentrations of GSH in 1.5 mL centrifuge tubes at room temperature. After the incubation of the required reaction time, the solutions were diluted to 250 μL in ultrapure water and mixed thoroughly. Afterwards, the mixtures were transferred into a 1 cm quartz cuvette and the fluorescence emission spectra were measured with excitation at 400 nm. The kinetic behaviors were studied by monitoring the fluorescence recovery of MnO_2 –SiQD nanocomposite by GSH in the different incubation time.

2.6. Cell culture, fluorescence imaging and cytotoxicity assay

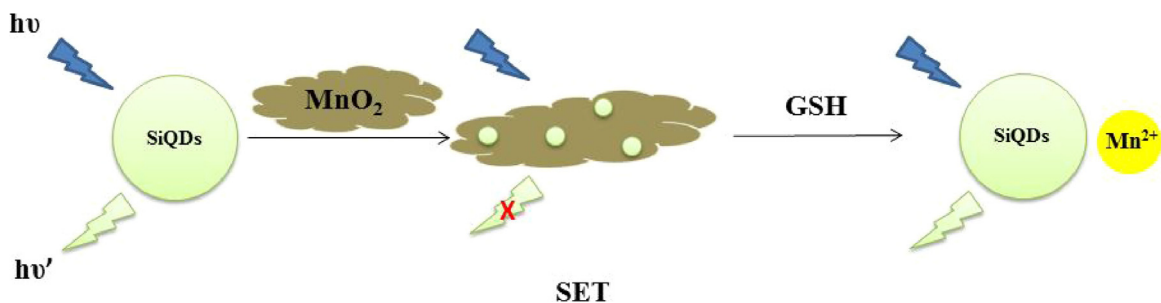
Cell culture and fluorescence imaging. Baby Hamster Syrian Kidney (BHK) cells were cultured in DMEM (Dulbecco's Modified Eagle Medium) supplemented with 10% FBS (fetal bovine serum). The cell lines were maintained in a humidified atmosphere containing 5% CO_2 at 37 °C. After removal of the culture medium, cells were incubated with MnO_2 –SiQD nanocomposite at desired concentrations in 1.0 mL of fresh culture medium for 4 h. Before imaging measurement, the cells were washed three times with phosphate buffer to remove the residual nanoparticles. Cells were observed under an Olympus FV1000-IX81 laser confocal microscope.

Cytotoxicity test. BHK cells were seeded at a density of 10^4 cells per well (100 μL total volume/well) in 96-well assay plates for 24 h. Then, the prepared MnO_2 –SiQD nanocomposite, at the indicated concentrations (0, 10, 20, 40, 60, 80 $\mu\text{g mL}^{-1}$), were added to the cell culture medium. Cells were incubated with MnO_2 –SiQD nanocomposite for 24 h. To determine toxicity, 3-(4,5-dimethylthiazol-2-yl)-5-(3-carboxymethoxyphenyl)-2-(4-sulfophenyl)-2*H*-tetrazolium, inner salts (MTS) was added to each well of the microtiter plate and the plate was incubated in the CO_2 incubator for additional 4 h. Absorbance values were determined with Bio-Rad model-680 microplate reader at 490 nm (corrected for background absorbance at 630 nm). The cell viability was estimated according to the following equation: cell viability (%) = mean of absorbance value of treatment group/mean absorbance value of control × 100%.

3. Result and discussion

3.1. Preparation and characterization of MnO_2 –SiQD nanocomposite

In this work, the SiQDs were synthesized by the previous method. The synthesized SiQDs are highly dispersible in water because of the amino group on the surface of SiQDs. MnO_2



Scheme 1. Schematic illustration of the design for GSH detection using MnO_2 -modified SiQDs.

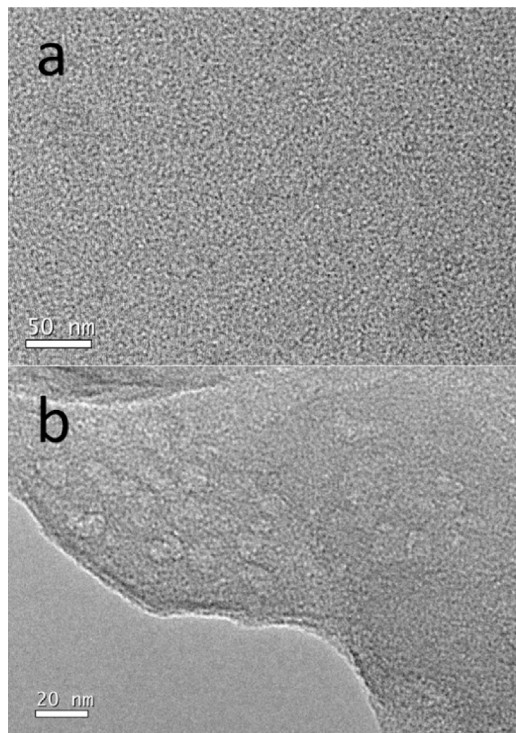


Fig. 1. TEM image of (a) SiQDs and (b) MnO_2 -SiQD nanocomposite.

nanosheets grew on the surface of the SiQDs by the addition of an aqueous solution of KMnO_4 in the presence of 2-(*N*-morpholino) ethanesulfonic acid (MES) buffer at pH 6. MnO_2 nanosheets were synthesized by reducing KMnO_4 in MES buffer. The formation of MnO_2 -SiQD nanocomposite assembles, dominated by electrostatic interactions, was characterized by TEM, DLS, XPS and FTIR.

Fig. 1 revealed the TEM images of the SiQDs and MnO_2 -SiQD. The TEM illustrates that the SiQDs are spherical and well dispersed, and have diameters of about 4 nm (Fig. 1a). Fig. 1b shows that spherical SiQDs loaded on wrinkle MnO_2 nanosheet. Importantly, the large surface area of MnO_2 nanosheet provides an essential platform for the reaction of trace amount of GSH and eventually benefits the high sensitivity of the probe. Also from the EDS element mapping data (Fig. S1), we can confirm that SiQDs are adhered to the surface of MnO_2 nanosheet. Dynamic light scattering (DLS) (Fig. S2) analysis shows the average hydrodynamic diameter of SiQDs is about 4 nm.

FT-IR and X-ray photoelectron spectroscopy (XPS) further provide the information of the successful deposition of the SiQDs on the surface of MnO_2 nanosheet. The FTIR spectrum of the SiQDs, MnO_2 and MnO_2 -SiQD nanocomposite are given in Fig. S3. From Fig. S3a, the band at 3379 cm^{-1} originates from the stretching vibration of N–H, while the band at 1573 cm^{-1} is assigned to

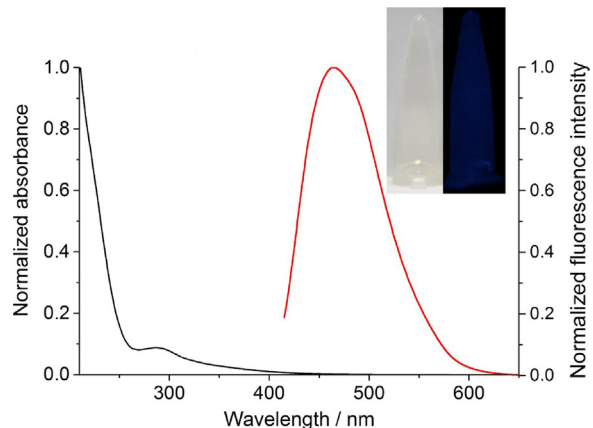


Fig. 2. Normalized UV-Vis (black) and steady-state fluorescence spectra (red, $\lambda_{\text{ex}} = 400\text{ nm}$) of SiQDs in water. Inset shows the SiQDs under daylight and UV light in water solution. (For interpretation of the references to color in this figure legend, the reader is referred to the web version of this article.)

N–H bending vibration. The peaks at 2928 cm^{-1} correspond to aliphatic C–H vibration, and the peak between 1132 and 1016 cm^{-1} is attributed to the Si–O stretching vibration. As shown in Fig. S3b, the broad band of MnO_2 at 3393 cm^{-1} should be attributed to the O–H stretching vibration, and 1634 , 1550 , 1367 and 1050 cm^{-1} bands are normally attributed to O–H bending vibrations. In the low frequency region, bands around 560 cm^{-1} should be ascribed to the Mn–O and Mn–O–Mn vibrations in $[\text{MnO}_6]$ octahedral [30]. From the comparison, it can be observed that the MnO_2 -SiQD nanocomposite contained the characteristic peaks of both prepared SiQDs and MnO_2 . SiQDs are attached on the surface of the MnO_2 nanosheet. In order to assess the successful attachment of SiQDs onto the surface of MnO_2 nanosheet, SiQDs and MnO_2 -SiQD nanocomposite were investigated by X-ray photoelectroscopic (XPS). The full-range SiQDs (Fig. S4a) spectrum depicts the binding energy peaks of Si 2p at 102.2 eV , C 1s at 285.1 eV , N 1s at 399.1 eV , O 1s at 532.1 eV . Compared to SiQDs, the XPS spectra of MnO_2 -SiQD nanocomposite in Fig. S4b show the peak at 642.4 eV was ascribed to Mn 2p, respectively. Obviously, these are important results which can confirm that the successful preparation of MnO_2 -SiQD nanocomposite.

Initial spectroscopic studies of SiQDs and MnO_2 nanosheets were undertaken by monitoring the UV-Vis absorption and fluorescence spectroscopy at room temperature. As shown in Fig. 2 (black), SiQDs exhibited an obvious absorption band centered at 288 nm and the optimal emission wavelength is 464 nm while the optimal excitation wavelength is 400 nm from Fig. 2 (red).

The change in the fluorescence emission spectra of this system centered at 464 nm as a function of $[\text{KMnO}_4]$ (MnO_2 nanosheets were prepared by reducing KMnO_4) was shown in Fig. 3. Upon the addition of KMnO_4 with increased concentration, SiQDs show a

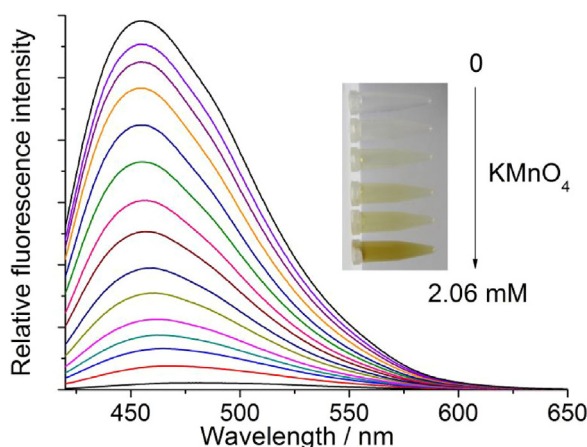
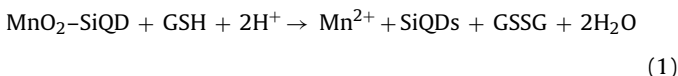


Fig. 3. Fluorescence emission spectra ($\lambda_{\text{ex}} = 400 \text{ nm}$) of SiQDs prepared by different concentrations of KMnO₄ in water. Inset shows that the solution color of the SiQDs turns gradually deep with the increase of KMnO₄ concentrations.

large decrease of the fluorescence intensity with a SET effect in the emission spectra and fluorescence quantum yield was observed. As seen from the inset of Fig. 3, the color of the solutions gradually changed from colorless to brown when KMnO₄ is added to the aqueous solution of SiQDs. Such changes of color and fluorescence were reasonably attributed to the formation of MnO₂–SiQD nanocomposite. When the concentration of MnO₂ nanosheets was higher than 1.57 mM, the maximum fluorescence quenching degree of the MnO₂–SiQD nanocomposite (Fig. 3) is up to 96%. The quantum yield of SiQDs decreases from 0.0400 ± 0.0015 in the absence of KMnO₄ to 0.0012 ± 0.0002 in addition of KMnO₄ up to 1.57 mM. Besides, as shown in Fig. S5, the fluorescence emission spectra have no obvious change when the MnCl₂ was added into the water solution of SiQDs.

3.2. Fluorescence response of MnO₂–SiQD nanocomposite towards GSH

MnO₂ in the proximity of SiQDs rendered the fluorescence of SiQDs in the Off state due to an efficient SET process. However, with the addition of GSH the fluorescence enhancement of SiQDs can be attributed to the reduction of MnO₂ to Mn²⁺, which is based on the unique reaction between GSH and MnO₂ nanosheet. During this redox reaction, GSH was oxidized to generate glutathione disulfide (GSSG) through thiol-disulfide exchange as shown in the following equation:



Fluorescence titration experiments were carried out to illustrate the emission response of MnO₂–SiQD nanocomposite to the various concentrations of GSH, as shown in Fig. 4a. The repeated experiment was taken for three times, and Fig. 4 showed the best one. With the concentration of GSH increased, the emission peak intensity at 464 nm of the sensing system increases monotonically. The restored fluorescence was dependent on the amount of GSH. When the concentration of GSH was increased to 1.57 mM, no further restoring of fluorescence can be observed, showing that the sensing response has reached the maximum. As can be seen from Fig. 4b, the fluorescence intensity increased almost linearly with increasing GSH concentration (13.3–417 μM). The calibration curve (Fig. 4c) for GSH concentrations was obtained as shown below, where ΔF

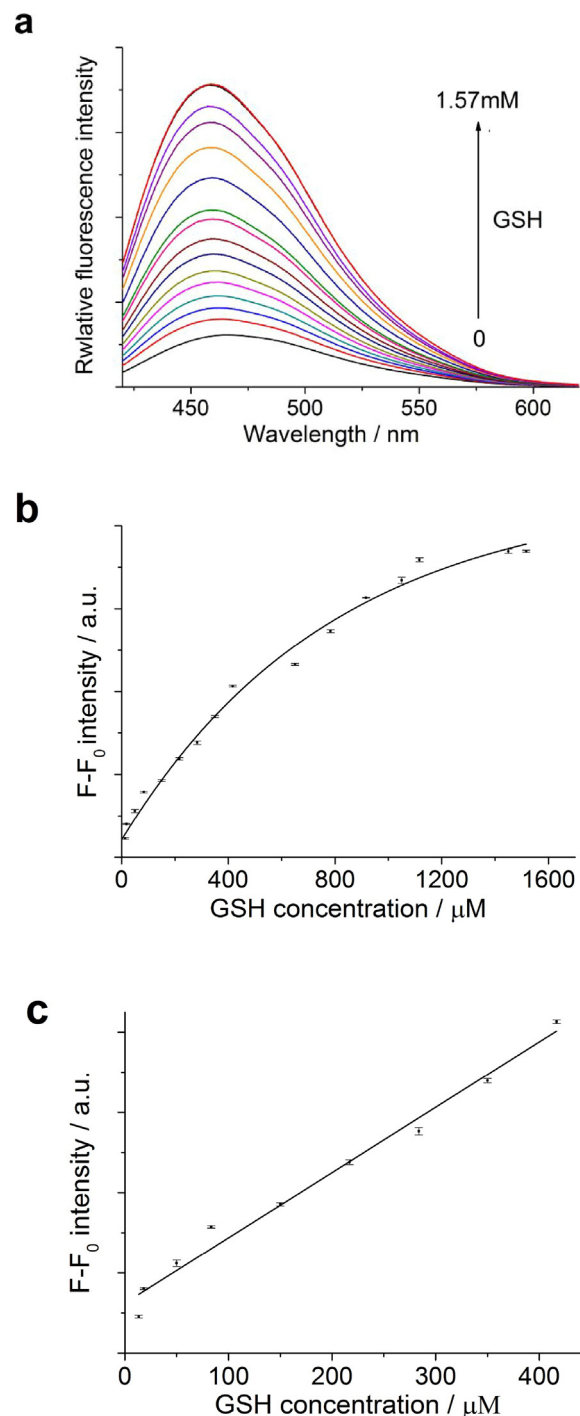


Fig. 4. (a) Fluorescence emission spectra ($\lambda_{\text{ex}} = 400 \text{ nm}$) of MnO₂–SiQD nanocomposite in the presence of different concentrations of GSH (0–1.57 mM). (b) Relationship between fluorescence enhancement and the target concentration. (c) Calibration curves between relative fluorescence intensity of MnO₂–SiQD and GSH concentration. F_0 represents the fluorescence intensity of MnO₂–SiQD without GSH, and F represents the fluorescence intensity with different GSH concentration ($\lambda_{\text{ex}} = 400 \text{ nm}$, $\lambda_{\text{em}} = 464 \text{ nm}$).

stands for the fluorescence enhancement against the concentration of GSH.

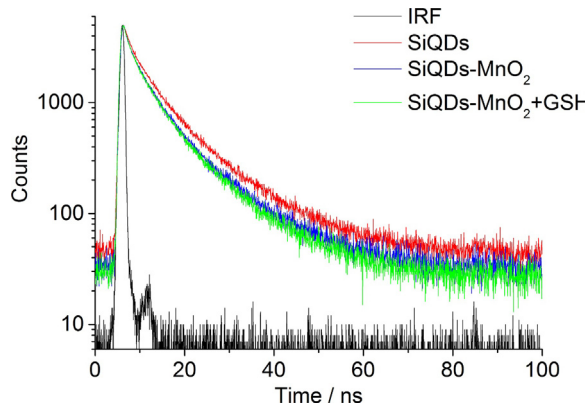
$$\Delta F = 249.2 + 3.253 \times [\text{GSH}] (r = 0.980, [\text{GSH}] = 13.3\text{--}417 \mu\text{M})$$

The calibration equation serves as the quantitative basis for the detection of GSH. The detection limit (DL) was estimated based on the following equation: $\text{DL} = 3\sigma/k$, where σ is the standard deviation

Table 1

Comparison of the method with others methods for GSH detection.

Method	Materials	Linear range (μM)	LOD (nM)	References
Fluorescent	Tetrafluoroterephthalonitrile (4F-2CN)	0–100	240	[8]
Fluorescent	CZ-Nm probe	0–10,000	6400	[3]
Fluorescent	A fluorescent probe including two potential reaction groups	20–500	430	[2]
Fluorescent	Rhodamine B-based fluorescent probe	0–80	189	[5]
Fluorescent	MnO_2 –SiQD nanocomposite	13.3–417	153	Our work

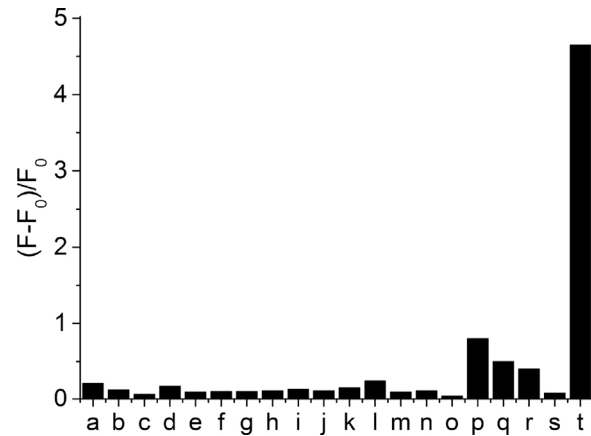
**Fig. 5.** Fluorescence decay profiles ($\lambda_{\text{ex}} = 400 \text{ nm}$ and $\lambda_{\text{em}} = 464 \text{ nm}$) of SiQDs, MnO_2 –SiQD and MnO_2 –SiQD with addition 1.57 mM GSH in aqueous suspension.

of the blank sample and k is the slope of the calibration curve. The DL of MnO_2 –SiQD nanocomposite was 153 nM. The result indicated that the MnO_2 –SiQD nanocomposite can be potentially utilized as an excellent optical sensor for the quantitative analysis of GSH in biological samples. As shown in Table 1, the detection limit obtained from this method was found to be lower or comparable than those of the others.

To investigate the fluorescence dynamics of SiQDs, fluorescence decay traces of SiQDs were recorded at 464 nm by the single-photon timing method [31]. Fluorescence decay for SiQDs water solution is fitted to the tri-exponential profile with the lifetime of $\sim 1.07 \text{ ns}$, $\sim 4.70 \text{ ns}$ and $\sim 12.7 \text{ ns}$ in water in the all fluorescence region, indicating that different energy levels lead to the formation of various radiative transitions. This can be attributed to the involvements of different emission trap sites present in the silicon core and on the surface [32]. Besides, SiQDs– MnO_2 nanocomposite also revealed tri-exponential behavior. The multi exponential nature of the lifetime suggests that the components of SiQDs in water are complicated, probably due to the involvement of different particle sizes and emissive trap sites.

Upon addition of 2.06 mM of KMnO_4 to aqueous solution of SiQDs, the fluorescence decay time does not change (Fig. 5). The measured lifetime in the presence of KMnO_4 is the same as the lifetime of the SiQDs in water. With the further increase of KMnO_4 concentration, the fluorescence decay time does not change either. A possible explanation for the fluorescence emission and lifetime changes of SiQDs with KMnO_4 is the surface energy transfer (SET) process. In the presence of KMnO_4 (MnO_2 nanosheets were prepared by reducing KMnO_4), the SET from the SiQDs (emission at about 464 nm) to the non-fluorescent MnO_2 nanosheets is enhanced. This enhancement in the SET induces quenching of the fluorescence as a function of KMnO_4 concentration.

The decrease of the fluorescence intensity with the increase of the concentration of KMnO_4 means that the concentration of the non-fluorescent MnO_2 –SiQD nanocomposite increases. The non-fluorescent MnO_2 –SiQD nanocomposite does not change the fluorescence emission maximum wavelength and the lifetime of the SiQDs.

**Fig. 6.** Selectivity of the MnO_2 –SiQD nanocomposite for GSH over other potential interferences (2 mM each; for bovine serum albumin: 1 mg mL^{-1}). (a) KCl, (b) NaCl, (c) MgSO_4 , (d) CoCl_2 , (e) NaSO_4 , (f) MnCl_2 , (g) CaCl_2 , (h) Tris 7.0, (i) HEPES, (j) phosphate buffer, (k) BSA, (l) Glu, (m) Gly, (n) Asp, (o) fructose, (p) ascorbic acid, (q) Hcy, (r) Cys, (s) GSH with *N*-methylmaleimide and (t) GSH. F_0 and F are the fluorescence intensity of the probe in the absence and presence of the target (GSH) or nontarget samples, respectively.

3.3. Selectivity of the fluorescence response of MnO_2 –SiQD nanocomposite to GSH

Except for the requirement of sensitivity, good specificity was also needed. The selectivity of MnO_2 –SiQD nanocomposite toward GSH was evaluated by screening its response to biological ions and amino acids. As shown in Fig. 6, under identical conditions, only the addition of GSH resulted in a significant optical change; no obvious increase in fluorescent intensity were observed upon addition of biological ions, amino acids and GSH with *N*-methylmaleimide (NMM) (a scavenger of GSH). Cysteine (Cys), homocysteine (Hcy), fructose and ascorbic acid can cause the fluorescent response to MnO_2 –SiQD nanocomposite. However, the content of these interferences in biological system is much lower than GSH. Therefore, the results demonstrated that the present fluorescent sensing platform possesses excellent selectivity for GSH determination, and therefore can be used as a fluorescence nanomaterial to detect of the human serum GSH without significant interference from small molecular thiols.

3.4. Intracellular imaging applications

Encouraged by the above results, studies were carried out to assess the use of MnO_2 –SiQD nanocomposite in fluorescence imaging of cellular thiols. BHK cells were incubated with the nanoprobe (0.2 mg mL^{-1}) at 37°C for 4 h and subsequently analyzed the results by using the confocal fluorescence microscope. A significant blue fluorescence image (Fig. 7, image II) is produced in the cytosol of the cell. When the cells are treated with 500 μM NMM for 30 min, the resulting confocal microscope image (Fig. 7, image III) displays an intense decrease of the fluorescence intensity because of a decrease in the GSH concentration. The results suggest that the nanoprobe can easily penetrate cell membranes and reacting with resident

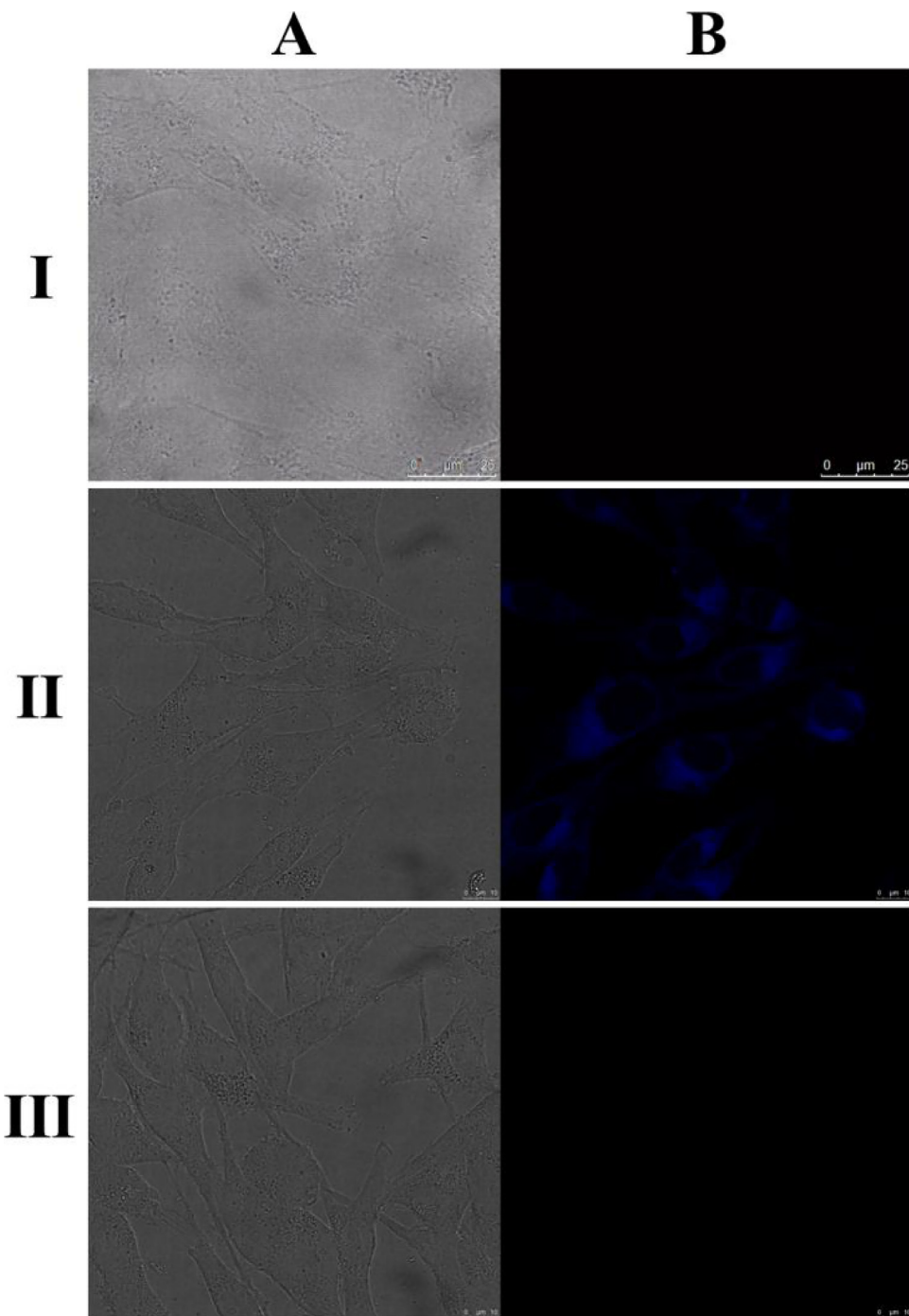


Fig. 7. Confocal fluorescence microscopy images of BHK cells (I) normal BHK cells, (II) cells incubated with $\text{MnO}_2\text{-SiQD}$ nanocomposite, (III) cells pretreated with NMM ($500 \mu\text{M}$) for 30 min, followed by $\text{MnO}_2\text{-SiQD}$ nanocomposite. Column A shows fluorescence microscopy images; column B shows the bright-field images.

thiols to produce discernible fluorescence images. Considering the relative high cytosolic concentration of GSH in cells and the relationship between the cytosolic GSH level with many diseases, this nanoprobe may offer a simple and visible way to control the cytosolic GSH level.

For intracellular imaging applications, the cytotoxicity of the nanoprobe is an important consideration. The cytotoxicity of $\text{MnO}_2\text{-SiQD}$ nanocomposite was evaluated by MTS assay in BHK cells. Fig. S6 shows the cell viability after incubation with $\text{MnO}_2\text{-SiQD}$ nanocomposite at a concentration of 0.20 mg mL^{-1} for 24 h. No significant reduction in cell viability was observed for cells treated with $\text{MnO}_2\text{-SiQD}$ nanocomposite even at high concentra-

tions (up to 0.20 mg mL^{-1}), demonstrating that the $\text{MnO}_2\text{-SiQD}$ nanocomposite produced in this study is of low toxicity in vitro.

4. Conclusion

In short, we have been successfully designed and synthesized a nanoprobe based on surface energy transfer from SiQDs to MnO_2 nanosheet and demonstrated its utility as a fluorescence turn-on nanoprobe which allows the selective detection of GSH in solution and in living cells. The recognition process involves that MnO_2 was reduced to Mn^{2+} and the fluorescence of SiQDs can be recovered in the presence of GSH. Confocal fluores-

cence microscopy experiments further demonstrated the utility of MnO₂–SiQD nanocomposite in monitoring GSH within living cells. This simple and cost effective method can be applied for the quantitative detection of GSH in living cells, for further understanding of its critical roles in the biological and pathological events.

Acknowledgments

This work was supported by the Ministry of Science and Technology of China (2014DFA31890). The authors would like to thank the National Natural Science Foundation of China (no. 21771092). This work was also supported by the State Key Laboratory of Veterinary Etiological Biology, Lanzhou Veterinary Research Institute, Chinese Academy of Agricultural Sciences.

Appendix A. Supplementary data

Supplementary data associated with this article can be found, in the online version, at <http://dx.doi.org/10.1016/j.snb.2017.08.170>.

References

- [1] G. Wu, Y.-Z. Fang, S. Yang, J.R. Lupton, N.D. Turner, Glutathione metabolism and its implications for health, *J. Nutr.* 134 (2004) 489–492.
- [2] Y. Li, W. Liu, P. Zhang, H. Zhang, J. Wu, J. Ge, et al., A fluorescent probe for the efficient discrimination of Cys, Hcy and GSH based on different cascade reactions, *Biosens. Bioelectron.* 90 (2017) 117–124.
- [3] L. Pang, Y. Zhou, E. Wang, F. Yu, H. Zhou, W. Gao, A “turn-on” fluorescent probe used for the specific recognition of intracellular GSH and its application in bioimaging, *RSC Adv.* 6 (2016) 16467–16473.
- [4] N. Shao, J. Jin, H. Wang, J. Zheng, R. Yang, W. Chan, et al., Design of bis-spiropyran ligands as dipolar molecule receptors and application to *in vivo* glutathione fluorescent probes, *J. Am. Chem. Soc.* 132 (2009) 725–736.
- [5] X. Wu, H. Shu, B. Zhou, Y. Geng, X. Bao, J. Zhu, Design and synthesis of a new rhodamine B-based fluorescent probe for selective detection of glutathione and its application for live cell imaging, *Sens. Actuators, B: Chem.* 237 (2016) 431–442.
- [6] J. Yin, Y. Kwon, D. Kim, D. Lee, G. Kim, Y. Hu, et al., Cyanine-based fluorescent probe for highly selective detection of glutathione in cell cultures and live mouse tissues, *J. Am. Chem. Soc.* 136 (2014) 5351–5358.
- [7] X. Zeng, X. Zhang, B. Zhu, H. Jia, W. Yang, Y. Li, et al., A colorimetric and ratiometric fluorescent probe for quantitative detection of GSH at physiologically relevant levels, *Sens. Actuators, B: Chem.* 159 (2011) 142–147.
- [8] H. Zhang, R. Liu, J. Liu, L. Li, P. Wang, S.Q. Yao, et al., A minimalist fluorescent probe for differentiating Cys, Hcy and GSH in live cells, *Chem. Sci.* 7 (2016) 256–260.
- [9] N.S. Lawrence, J. Davis, R.G. Compton, Electrochemical detection of thiols in biological media, *Talanta* 53 (2001) 1089–1094.
- [10] O. Nekrassova, P.C. White, S. Threlfall, G. Hignett, A.J. Wain, N.S. Lawrence, et al., An electrochemical adaptation of Ellman's test, *Analyst* 127 (2002) 797–802.
- [11] A. Safavi, N. Maleki, E. Farjami, F.A. Mahyari, Simultaneous electrochemical determination of glutathione and glutathione disulfide at a nanoscale copper hydroxide composite carbon ionic liquid electrode, *Anal. Chem.* 81 (2009) 7538–7543.
- [12] Y. Hiraku, M. Murata, S. Kawanishi, Determination of intracellular glutathione and thiols by high performance liquid chromatography with a gold electrode at the femtomole level: comparison with a spectroscopic assay, *Biochim. Biophys. Acta* 1570 (2002) 47–52.
- [13] B.A. Neuschwander-Tetri, F.J. Roll, Glutathione measurement by high-performance liquid chromatography separation and fluorometric detection of the glutathione-orthophthalaldehyde adduct, *Anal. Biochem.* 179 (1989) 236–241.
- [14] D.M. Townsend, K.D. Tew, H. Tapiero, The importance of glutathione in human disease, *Biomed. Pharmacother.* 57 (2003) 145–155.
- [15] J. Fan, Z. Wang, H. Zhu, N. Fu, A fast response squaraine-based colorimetric probe for detection of thiols in physiological conditions, *Sens. Actuators, B: Chem.* 188 (2013) 886–893.
- [16] Y. Li, P. Wu, H. Xu, H. Zhang, X. Zhong, Anti-aggregation of gold nanoparticle-based colorimetric sensor for glutathione with excellent selectivity and sensitivity, *Analyst* 136 (2011) 196–200.
- [17] M. Shamsipur, A. Safavi, Z. Mohammadpour, Indirect colorimetric detection of glutathione based on its radical restoration ability using carbon nanodots as nanozymes, *Sens. Actuators, B: Chem.* 199 (2014) 463–469.
- [18] S. Banerjee, S. Kar, J.M. Perez, S. Santra, Quantum dot-based OFF/ON probe for detection of glutathione, *J. Phys. Chem. C* 113 (2009) 9659–9663.
- [19] D. Tian, Z. Qian, Y. Xia, C. Zhu, Gold nanocluster-based fluorescent probes for near-infrared and turn-on sensing of glutathione in living cells, *Langmuir* 28 (2012) 3945–3951.
- [20] Q.-Y. Cai, J. Li, J. Ge, L. Zhang, Y.-L. Hu, Z.-H. Li, et al., A rapid fluorescence “switch-on” assay for glutathione detection by using carbon dots–MnO₂ nanocomposites, *Biosens. Bioelectron.* 72 (2015) 31–36.
- [21] F. Erogogbo, K.-T. Yong, I. Roy, G. Xu, P.N. Prasad, M.T. Swihart, Biocompatible luminescent silicon quantum dots for imaging of cancer cells, *ACS Nano* 2 (2008) 873–878.
- [22] Y. He, Y. Su, X. Yang, Z. Kang, T. Xu, R. Zhang, et al., Photo and pH stable, highly-luminescent silicon nanospheres and their bioconjugates for immunofluorescent cell imaging, *J. Am. Chem. Soc.* 131 (2009) 4434–4438.
- [23] K. Sato, S. Yokosuka, Y. Takigami, K. Hirakuri, K. Fujioka, Y. Manome, et al., Size-tunable silicon/iron oxide hybrid nanoparticles with fluorescence, superparamagnetism, and biocompatibility, *J. Am. Chem. Soc.* 133 (2011) 18626–18633.
- [24] K.M. Ainslie, S.L. Tao, K.C. Popat, T.A. Desai, In vitro immunogenicity of silicon-based micro-and nanostructured surfaces, *ACS Nano* 2 (2008) 1076–1084.
- [25] Z. Xu, D. Wang, M. Guan, X. Liu, Y. Yang, D. Wei, et al., Photoluminescent silicon nanocrystal-based multifunctional carrier for pH-regulated drug delivery, *ACS Appl. Mater. Interfaces* 4 (2012) 3424–3431.
- [26] Z. Kang, C.H.A. Tsang, N.-B. Wong, Z. Zhang, S.-T. Lee, Silicon quantum dots: a general photocatalyst for reduction, decomposition, and selective oxidation reactions, *J. Am. Chem. Soc.* 129 (2007) 12090–12091.
- [27] M. Shao, H. Wang, M. Zhang, D. Duo Duo Ma, S.-T. Lee, The mutual promotional effect of Au–Pd bimetallic nanoparticles on silicon nanowires: a study of preparation and catalytic activity, *Appl. Phys. Lett.* 93 (2008) 243110.
- [28] B. Xia, W. Zhang, J. Shi, S. Xiao, Fluorescence quenching in luminescent porous silicon nanoparticles for the detection of intracellular Cu²⁺, *Analyst* 138 (2013) 3629–3632.
- [29] J. Wang, D.-X. Ye, G.-H. Liang, J. Chang, J.-L. Kong, J.-Y. Chen, One-step synthesis of water-dispersible silicon nanoparticles and their use in fluorescence lifetime imaging of living cells, *J. Mater. Chem. B* 2 (2014) 4338–4345.
- [30] H.-Y. Chu, Q.-Y. Lai, L. Wang, J.-F. Lu, Y. Zhao, Preparation of MnO₂/WMT composite and MnO₂/AB composite by redox deposition method and its comparative study as supercapacitive materials, *Ionics* 16 (2010) 233–238.
- [31] N. Boens, W. Qin, N. Basaric, J. Hofkens, M. Ameloot, J. Pouget, et al., Fluorescence lifetime standards for time and frequency domain fluorescence spectroscopy, *Anal. Chem.* 79 (2007) 2137–2149.
- [32] B. Li, Y. Guo, A. Iqbal, Y. Dong, W. Li, W. Liu, et al., Insight into excitation-related luminescence properties of carbon dots: synergistic effect from photoluminescence centers in the carbon core and on the surface, *RSC Adv.* 6 (2016) 107263–107269.

Biographies

Hong Ma received his B.E. degree from University of Electronic Science and Technology of China, PR China, in 2015. He is currently a master candidate at College of Chemistry and Chemical Engineering, Lanzhou University, PR China. His research interests focus on developing fluorescent chemosensors.

Xinran Li received his MASTER degree from Lanzhou Jiaotong University, PR China, in 2014. He is currently a Ph.D. scholar at College of Chemistry and Chemical Engineering, Lanzhou University, PR China. His research interests focus on developing fluorescent chemosensors.

Xiaoyu Liu obtained her Ph.D. degree from Lanzhou University, PR China, in 2016. Then, she joined Lanzhou University of Technology as a lecturer. Her research interests focus on developing fluorescent chemosensors.

Min Deng received her B.S. degree from Lanzhou University, PR China, in 2014. She is currently a master candidate at College of Chemistry and Chemical Engineering, Lanzhou University, PR China. Her research interests focus on developing fluorescent chemosensors.

Xudong Wang received his B.S. degree from Qingdao University of Science & Technology, PR China, in 2013. He is currently a master candidate at College of Chemistry and Chemical Engineering, Lanzhou University, PR China. His research interests focus on developing fluorescent chemosensors.

Anam Iqbal received her MASTER degree from University of Balochistan Quetta, Pakistan in 2006, Worked as a Lecture in University of Balochistan Quetta, Pakistan. She is currently a Ph.D. scholar at College of Chemistry and Chemical Engineering, Lanzhou University, PR China. Her research interests focus on fluorescent chemosensors.

Weisheng Liu received his Ph.D. degree from Lanzhou University, PR China, in 1996. He is currently a professor at College of Chemistry and Chemical Engineering, Lanzhou University, PR China. His research interests focus on developing function materials and fluorescent chemosensors.

Wenwu Qin received his Ph.D. degree from Lanzhou University, PR China, in 2003. He is currently a professor at College of Chemistry and Chemical Engineering, Lanzhou University, PR China. His research interests focus on developing fluorescent chemosensors.